Microscopic insights into thermal cycling effects in granular materials via X-ray microtomography

Yize Pan[1], Dawa Seo[1], Mark Rivers[2], Xiaohui Gong[1], Giuseppe Buscarnera[1], and Alessandro F. Rotta Loria[1*]

[1] *Department of Civil and Environmental Engineering, Northwestern University, 2145 Sheridan Road, Evanston, Illinois 60208, USA*

[2] *Center for Advanced Radiation Sources, University of Chicago, 9700 South Cass Avenue, Argonne, IL 60647*

[*]Corresponding author: af-rottaloria@northwestern.edu

Abstract

The mechanics of granular materials at the macroscopic scale inherently depends on the particle interactions occurring at the microscopic scale. In recent decades, growing investigations have explored the mechanics of granular materials subjected to thermal cycles, as they involve complex responses that bear significance for science, engineering, and technology. However, the fundamental understanding of the mechanics of granular materials subjected to thermal cycles remains hindered by the absence of empirical evidence into the microscopic particle interactions that govern the macroscopic response of such materials. For the first time, this study presents direct experimental evidence obtained via synchrotron X-ray microtomography to reveal the behavior of the particles that constitute granular materials during thermal cycling. This work experimentally confirms the existing theory by which thermally induced particle interactions drive a macroscopic volumetric expansion and contraction of granular materials upon heating and cooling, respectively, and the development of irreversible volumetric deformations upon the completion of thermal cycles. The results uncover the evolution of particle non-uniform translations, rotations, and contact variations during thermal cycling, which all inherently depend on particle shape.

Keywords: granular materials; mechanics; temperature variations; thermal cycling; tomography

1. Introduction

Granular materials, such as sands and beads, are widely encountered in both natural and engineered systems. Despite being composed of particles with simple properties and behaviors, these materials exhibit a wide range of distinct properties and behaviors that are significantly more complex compared to those of their constituting particles [1–3]. The complexity of granular materials arises from intricate microscopic particle interactions [4], which vary depending on variables such as particle shape [3, 5, 6] and gradation [7].

Over the past decades, the mechanics of granular materials subjected to temperature variations has garnered substantial interest across fundamental and applied science, owing to its complexity and potential impact on the performance of engineering and technological solutions [8–31]. Early experimental studies primarily focused on the mechanics of sands under monotonic temperature variations exceeding 100°C [8–10]. These studies aimed to evaluate the potential changes in sand properties due to extreme temperatures, which could influence the extraction of deep geological resources [32]. Subsequent experimental and computational investigations delved deeper into the response of sands to monotonic temperature variations [19], exploring their response to a single cycle of heating and cooling [18, 26, 28, 29], as well as multiple cycles of heating and cooling [23, 31]. The primary objective of these studies has been to gather comprehensive insights into the mechanics of sands subjected to temperature variations. Multiple investigations have explored the residual effects of cyclic temperature variations on the mechanics of granular materials, particularly spherical beads [9, 11–17, 20–22, 24, 25, 27]. The focus on multiple thermal cycles is driven by their relevance to packed-bed thermal energy storage systems, where granular materials are subjected to repeated heating and cooling. These studies have shown that thermal cycling can result in irreversible volumetric deformations, which can affect the performance of these applications [34, 35]. Generally, the irreversible deformations of granular materials due to thermal cycling have been shown to be contractive [11–13, 16, 17, 20–22, 24, 27], but evidence has also presented expansive residual deformations [17], depending on the initial state of the granular packing. The deformations caused by thermal cycling have been noted to involve effects comparable to those of vibration [11, 13, 36], although their origin is clearly different. Whether these deformations can be formally attributed to a ratcheting behavior (i.e., the continued net accumulation of irreversible deformations with successive loading cycles [37]) or a plastic shakedown behavior (i.e., the gradual reduction of cumulative irreversible deformations due to cyclic loading, which stabilize as the number of applied cycles approaches infinity [38]) still represents an open question. The reason for this uncertainty is that deformations caused by thermal cycling do not always appear to stabilize over successive cycles [11–13, 16, 17, 20–22, 24, 27]. Computational studies free from experimental artifacts that potentially lead to continued accumulation of irreversible deformations due to successive cyclic loading [39] still observe the ratcheting phenomenon [22]. This phenomenon is attributed to the creation of permanent convection cells, as observed in granular materials subjected to cyclic mechanical loading [40]. In contrast, other numerical studies observe a stabilization of the irreversible deformations caused by successive thermal cycles [27], indicating a thermal plastic shakedown also recently observed in experimental studies on sands [31]. Notably, the application of cyclic mechanical loads on sands has also been attributed to a plastic shakedown behavior, rather than a ratcheting behavior [41].

As most studies explored the residual effects of thermal cycling after the application, rather than focusing on the response of granular materials during monotonic heating or cooling, the knowledge of the response of granular materials to heating or cooling remains limited. The available studies have primarily focused on sands within the context of geothermal applications [8, 19, 26, 30, 32]. Although some experimental observations have indicated macroscopic volumetric contractions of sands upon heating [8, 10, 18, 23, 28], such observations have been attributed to measurement inaccuracies [29, 30]. In alignment with this assessment, experiments benefiting from accurate and controlled measurement conditions have consistently indicated macroscopic volumetric expansions and contractions of sands upon heating and cooling, respectively [19, 26, 30]. These latter observations appear to reflect the macroscopic constitutive behavior of sands more rationally. However, more studies (e.g., experimental) are deemed essential to develop a comprehensive set of evidence regarding the influence of temperature variations on sands and other granular materials.

The existing state-of-the-art highlights the need for additional studies to develop a comprehensive and consistent understanding on the mechanics of granular materials. Meanwhile, an analysis of the available studies enables the identification of a critical gap in the literature: the lack of experimental investigations providing microscopic insights into how fundamental particle interactions govern the mechanics of granular materials subjected to temperature variations, particularly their interconnected thermally induced deformations during and after the application of thermal cycles. In this context, the following questions emerge: How do granular particles translate and rotate in space when subjected to temperature variations? How uniform are these particle movements, and how do they influence the coordination number in granular materials? What is the influence of particle shape on all these microscopic phenomena? This paper addresses these questions by leveraging recent technological advancements in X-ray computed tomography (CT) [42, 43], which have opened up new avenues for microstructural investigations about the mechanics of granular materials.

Specifically, this study presents the first temperature-controlled tomography experiments and image analyses aimed at visualizing and monitoring the microstructure of granular materials in response to thermal cycles, focusing on the influence of both monotonic and cyclic temperature variations. This endeavor is performed with a focus on sands, as they emerge for their particularly complex particle shapes. With these premises, this study presents tomography experiments on two types of dry silica sands with rounded and angular particle shapes. Using a custom-designed sample cell with temperature control, the study explores the behavior of such materials under laterally restrained and free head conditions in a cylindrical container. Each studied sample consists of over 1200 particles and is subjected to five thermal cycles with a temperature variation of $\Delta\bar{T} = 100$°C. Three-dimensional (3-D) CT images are captured at each temperature step after achieving thermal stabilization. Subsequently, image analyses are performed to quantify microstructural changes, including particle volumes changes, translations, rotations, and contacts. This study crucially discusses the obtained results and advances toward a more comprehensive and mechanistic understanding of the mechanics of granular materials under non-isothermal conditions.

2. Materials and methods

2.1 Experimental apparatus

The experiments presented in this study were conducted at the synchrotron microtomography facility of Sector 13-BM-D GeoSoilEnviroCARS (GSECARS) located at the Advanced Photon Source, Argonne National Laboratory. The pink beam tomography technique [43] was utilized to acquire high-resolution X-ray CT images with a spatial resolution of 3.13 μm per voxel. These images enable precise quantitative analyses of the microstructure at the level of individual particles. The temperature within the tomography room was maintained constant at 23.5 ± 1°C throughout the experiments. Further details of the beamline facility and experimental setup utilized in this study can be found elsewhere [44], and a brief summary is presented here.

Each image set required the combination of three image sections collected at three different heights. At each height, the sample needed to be rotated 180° at acquisition speed to collect the projections required for 3-D reconstruction. In addition, the sample needed to be moved horizontally out of the view at each height to collect the flat field for image correction. Very slow speeds and long acceleration times [44] were used to minimize the disturbances during horizontal, vertical, and rotational movements. The parameters of scanning movements adopted for image collection are comprehensively reported elsewhere [44].

Calibration tests where a rounded sand sample was scanned 13 times at room temperature showed minimal disturbances (maximum particle translation < 4 μm) from scanning movements.

Temperature-controlled tomography experiments were performed under laterally restrained conditions and zero applied vertical stress at the head of samples located in a cylindrical container (Figure 1). The sample container was made of fused quartz due to its low X-ray attenuation and very low thermal expansion coefficient (linear thermal expansion coefficient of 5.5×10^{-7} 1/°C). This ensured minimal variations in the lateral restraint provided to the sample under non-isothermal conditions. The container with one flat closed end had an inside diameter of 5 mm, an outside diameter of 7 mm, and an inside height of 10 mm. The open top prevented the build-up of excess air pressure due to thermal expansion that may cause particle movements. To hold the container at the base, one single set screw was used. A high-temperature polymer cell was built by 3-D printing to provide thermal insulation. A stream of nitrogen gas was blown from the top ceramic tube, which contained an electric resistance heater to heat the gas stream. The power output to the heater was regulated by a PID temperature controller, adjusting the control voltage to achieve different heating rates and temperature setpoints. The feedback temperature was read from a thermocouple attached to the sample cylinder at the base.

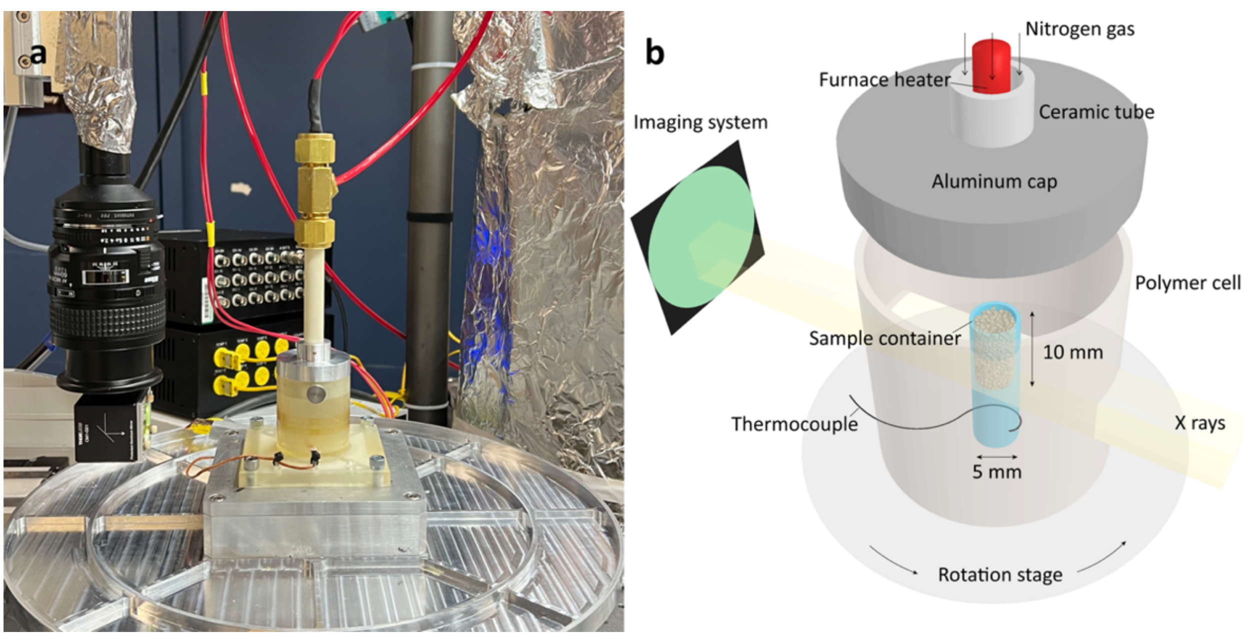

Figure 1: Experimental setup. The sample is scanned in a temperature-controlled cell. (a) Global view of the setup. (b) Detailed schematic with descriptions.

2.2 Test materials

The materials used in this study were two types of dry silica sand: a rounded F-35 sand (Ottawa, IL) and an angular 1 Q-ROK sand (Berkeley Springs, WV), both composed of over 99% quartz. Their original particle size distributions are very similar and the particle shape characterizations are presented elsewhere [31]. The two types of sand were artificially sieved to their mean sizes, both between No. 30 (600 μm) and No. 40 (425 μm) sieves. Loose samples were prepared using the air-pluviation method [45] (i.e., by raining uniformly the material into the container). The container was filled below the top, at a height of around 9 mm, to avoid potential overflow during thermal expansion. The experiments were performed using 1380 rounded particles with an initial average porosity of 0.43, and 1250 angular particles with an initial average porosity of 0.54.

2.3 Temperature calibration

Temperature calibration test was performed to understand the correlation between the actual sample temperature and feedback temperature. In addition to a feedback thermocouple used for measuring feedback temperature in the setup shown in Figure 1, an additional thermocouple was inserted into the sand sample (reaching the bottom of the cylinder) to measure the sample temperature (Figure 2(a)) during the temperature calibration test. The results indicate that the sample temperature was highly responsive to the change in control voltage regulated by the PID controller, since the sample was in closer proximity to the heat source compared to the feedback thermocouple (Figure 2(b)). Despite the feedback temperature being nearly synchronized with the setpoint upon heating, the sample temperature was raised much higher than the feedback temperature. When the heating rate was set at 0.1°C/s, the sample temperature overshot significantly beyond the feedback temperature followed by cooling down towards thermal stabilization. Using a lower heating rate of 0.02°C/s allowed to significantly reduce the overshoot and was therefore preferred for temperature uniformity and stabilization. A nearly linear correlation between the sample temperature and feedback temperature at thermal stabilization was observed (see the inset in Figure 2(b)). Cooling was achieved by turning off the heater and blowing gas at room temperature. The sample temperature initially dropped rapidly and became almost synchronized with the feedback temperature towards stabilization at room temperature.

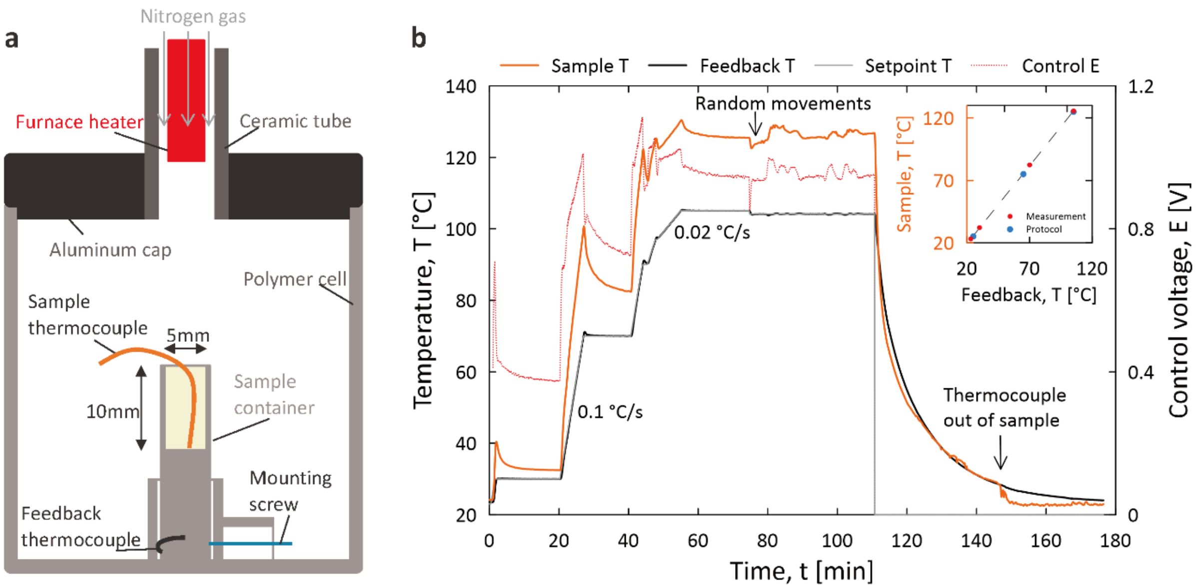

Figure 2: Temperature calibration. (a) Cross-section schematic of the set-up for temperature calibration. The feedback thermocouple is attached to the cylinder base to measure the feedback temperature, which was used to provide feedback and control the PID controller regulating the control voltage to the heater. To calibrate the correlation between the actual sample temperature and the feedback temperature, an additional thermocouple was inserted into sand particles in the sample container to measure sample temperature. (b) Temperature and voltage readings during the temperature calibration test. Different heating rates were applied to the setpoint. The value of the control voltage indicates the level of power output to the heater. The term "random movement" refers to the movement of the stage, typical for CT scanning to collect 3-D images, which results in fluctuations in the readings of the thermocouples due to varying contact with the hot gas. The correlation between sample temperature and feedback temperature at thermal stabilization is shown in the upper right corner, where the red dots represent measurements from the calibration, and the blue dots represent the temperatures applied in the actual test protocol.

2.4 Test protocol

Based on the results of the temperature calibration, a refined temperature protocol was developed for the actual tests (Figure 3). Five thermal cycles with an average sample temperature amplitude of 100°C were applied to both sand samples, showing consistent results. The chosen temperature amplitude of 100°C characterizes granular materials such as sands in engineered systems used for high-temperature thermal energy storage or in natural systems including deserts on the Moon and Mars. The first thermal cycle consisted of two steps for both heating and cooling, while the subsequent four thermal cycles involved only one step for both heating and cooling. Images were collected after reaching thermal stabilization at each temperature step. One image set, consisting of three image sections, was collected in approximately 10 minutes.

To compensate for the correlation between the sample and feedback temperatures, a feedback temperature step of 40 or 80°C was applied to achieve a sample temperature step of 50 or 100°C. The feedback temperature was initially set at 25°C and increased to 105°C to reach a sample temperature of 125°C. To minimize overshoot, each heating step consisted of two phases: a fast-heating phase and a slow-stabilizing phase. The fast-heating phase, which accounts for 5/8 of the step, used a setpoint heating rate of 0.1°C/s to accelerate the experiment within the limited beamtime. The slow-stabilizing phase, referring to the remaining 3/8 of the step, used a heating rate of 0.02°C/s to minimize temperature overshoot. Heating up by 100°C took approximately 40 minutes. Cooling was simpler and less concerned with overshoot, except for the first cycle which had two cooling steps. A 100°C drop in temperature took about 70 minutes.

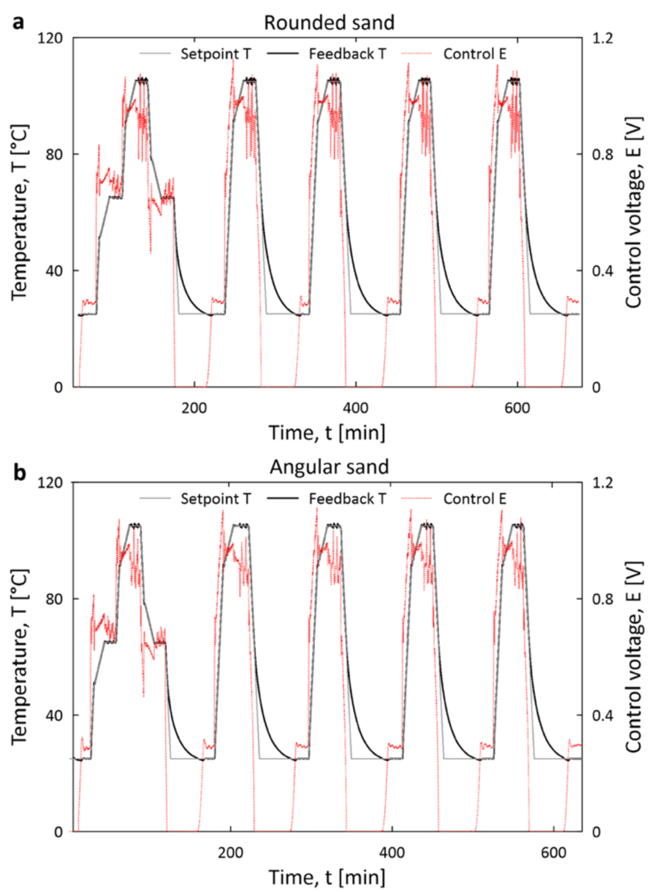

Figure 3: Test protocol for actual tests where five thermal cycles were applied on sand samples. As shown in the upper right corner of Figure 2(b), a feedback temperature step of 40 or 80°C was applied to achieve a sample temperature step of 50 or 100°C. The feedback temperature was initially set at 25°C and increased to 105°C during heating to reach a sample temperature of 125°C. (a) Temperature and voltage readings during the test on rounded particles. (b) Temperature and voltage readings during the test on angular particles

2.5 Image analyses

Image analyses were conducted on the image sets acquired from the tomography experiments. These analyses are carried out in four phases: image reconstruction using IDL, image processing using Avizo, particle tracking, and microstructural analyses using Matlab. The first three phases are discussed in detail elsewhere [44], while the microstructural analyses focusing on particle volumes, translations, rotations, and contacts are described hereafter.

2.5.1 Particle volume changes and temperatures

Temperature variations generate volume changes in granular particles due to their thermal expansion and contraction. Specifically, thermally induced strains are inherently related to applied temperature variations. In the experiments, the volume change of each individual particle was quantified. Accordingly, it was possible to use the probed particle volume changes to approximately infer the temperature variations that characterize the individual particles. This analysis is indeed approximate and can only provide qualitative information about particle temperatures, mainly because individual particles undergoing temperature variations in a packing are not able to deform freely (i.e., they are at least partly constrained). As a result, the particle temperatures inferred in this manner are likely smaller than the actual particle temperatures that develop in reality. Additionally, the image resolution was not sufficient to quantify the volume change of each particle due to temperature variations at the order of 1°C (a resolution of nanometers is necessary). However, analyses relying on the statistics of over 1200 particles tested in the various experiments provided qualitative yet valuable information about the influence of a temperature variation of 100°C.

2.5.2 Particle translations

Particle translations were analyzed by referring to the X, Y, Z coordinates of the center of each particle (Figure 4). To ensure a consistent reference for the origin and axis directions, the coordinate system was set up and corrected for every calculation. This approach was necessary because the movement and tilt of the sample cylinder are inevitable due to thermal expansion of the system. The origin centering and tilt correction of the coordinate system were performed based on the positions and movements of the bottom layer particles, as described in detail elsewhere [44]. The approach of centering the coordinate origin at the center of over 50 particles in the bottom layer has proven effective in providing a reliable reference and efficiently handling the computational demands of the analysis.

Centering the coordinate origin at the center of over 50 particles in the bottom layer has proven effective in providing a reliable reference and efficiently handling the computational demands of the analysis. Once a consistent coordinate system was established, particle translations were calculated by subtracting their X, Y, Z coordinates between each two image sets. Upward particle translations and expansive strains are considered positive in this study.

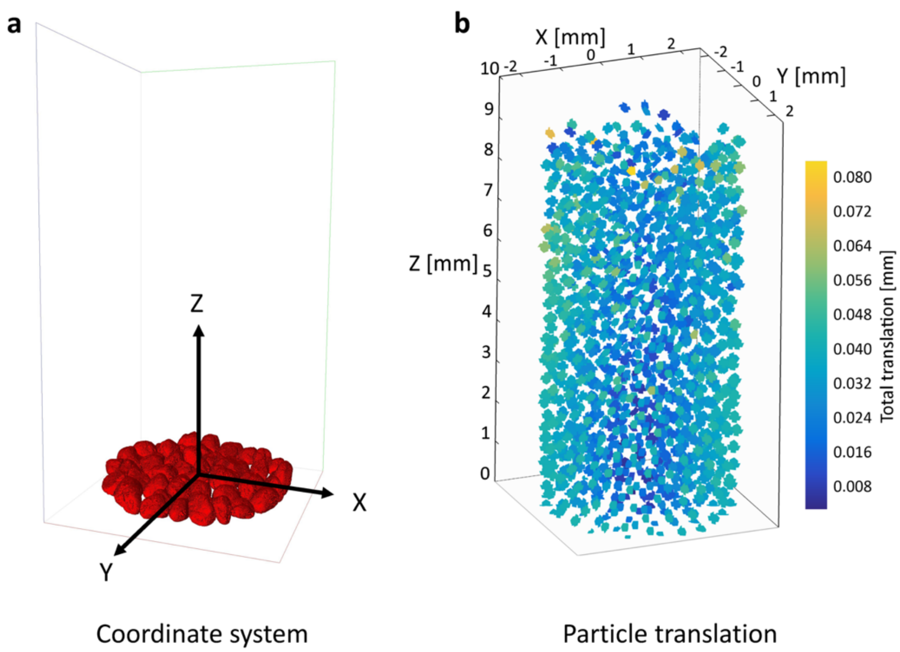

Figure 4: Particle translation calculation. (a) The origin of coordinate system is set at the center of the bottom layer particles and corrected for cylinder tilt. (b) Visualized illustration of traced translations of rounded sand particles induced by five thermal cycles. The detailed quantifications of particle vertical translations are presented in subsequent sections.

Given the considered setup of image resolution and sample size, three image sections were stitched together to generate a complete image of the entire sample. During this process, some voxels around the image stitches may have been missed or duplicated, particularly if the stage position control encountered minor deviations. When the temperature was significantly raised, the thermal expansion of the machinery below not only caused the lifting of the sample within the field of view, but also had the potential to exacerbate the stage positioning deviations. As a result, artifacts such as variations in particle volumes and centroid locations of particles at the stitches may have been introduced, leading to possible shifts of the slopes of the particle vertical translations. Fortunately, these artifacts were only noticeable when considering images with a large temperature difference, whereas they were negligible when comparing images at a consistent temperature (e.g., 25°C).

2.5.3 Thermoelastic displacements

To facilitate the analyses of particle translations upon monotonic heating and cooling, thermoelastic displacements were derived from the measured particle volume statistics, as well as from the theoretical volumetric and linear thermal expansion coefficients of the solid particles. The following complementary methods were employed to compare with actual particle vertical translations.

First, thermoelastic displacements were calculated from the statistics of measured particle volume changes in the CT images. These displacements were calculated assuming one-dimensional displacements with no reorganizations as follows:

$$\Delta Z^{th} = H \sum_{h=0}^{H} \Delta V_s^{m} \,/\, \sum_{h=0}^{H} V_{s,i}^{m} \tag{1}$$

where $\sum_{h=0}^{H} \Delta V_s^{m}$ and $\sum_{h=0}^{H} V_{s,i}^{m}$ are the summations of volume changes and initial volumes of individual particles located below a given initial height H (when comparing two image sets), respectively.

Second, thermoelastic displacements were calculated from the theoretical volumetric thermal expansion of alpha quartz. The rate of volume change due to thermal expansion of sand particles can be expressed as $dV_s = \beta(T) V_s dT$, where $\beta(T)$ is the theoretical volumetric thermal expansion coefficient. Exact integration provides the theoretical volume change with reference to the initial volume $\Delta V_s^{th}/V_{s,i} = \exp\left(\int_{T_i}^{T_f} \beta(T) dT\right) - 1$. Therefore, displacements were calculated from the volumetric thermal expansion of the particles as follows:

$$\Delta Z_v^{th} = H \left[\exp\left(\int_{T_i}^{T_f} \beta(T) dT\right) - 1\right] \tag{2}$$

Finally, thermoelastic displacements were calculated from the theoretical linear thermal expansion of alpha quartz. A simplified average was considered in this study to account for the varying linear thermal expansion coefficients along different axes of the crystal structure of alpha quartz. Therefore, displacements associated with the linear thermal expansion of the particles were obtained as:

$$\Delta Z_l^{th} = \Delta Z_v^{th}/3 \tag{3}$$

Rather than assuming a constant value for the volumetric thermal expansion coefficient, which is used in the reference formulations of the displacements expressed in equations (2) and (3), the calculations accounted for a temperature-dependent thermal expansion coefficient to provide more accurate results [46]. Given the crystal structure of alpha quartz, the volumetric thermal expansion $\beta(T)$ was calculated as $\beta = 2\alpha_s^a + \alpha_s^c$. Here, α_s^a represents the linear thermal expansion coefficient along the a-axis and α_s^c represents the one along the c-axis. Their values were determined by the 5th order polynomial expression provided by Kosinski et al. [47] within the temperature range of -50 °C to 150 °C. The expression of $\beta(T)$ is given by:

$$\beta(T) = a_0 + a_1 T + a_2 T^2 + a_3 T^3 + a_4 T^4 + a_5 T^5 \quad (4)$$

with $a_0 = 3.33 \cdot 10^{-5}$ 1/°C, $a_1 = 6.94 \cdot 10^{-8}$ 1/°C^2, $a_2 = -1.667 \cdot 10^{-10}$ 1/°C^3, $a_3 = -6.094 \cdot 10^{-13}$ 1/°C^4, $a_4 = 6.473 \cdot 10^{-15}$ 1/°C^5, $a_5 = -1.304 \cdot 10^{-17}$ 1/°C^6.

During the heating process from an initial temperature $T_i = 25$ °C and a final temperature $T_f = 125$ °C, an equivalent $\beta^{eq} = \frac{\exp\left(\int_{T_i}^{T_f} \beta(T) dT\right) - 1}{T_f - T_i} = 3.74 \times 10^{-5}$ 1/°C is obtained. Therefore, an equivalent $\alpha^{eq} = \beta^{eq}/3 = 1.25 \times 10^{-5}$ 1/°C is obtained. These values are considered as reference for this study.

2.5.4 Particle rotations

To detect particle rotation, the orientation of each particle was analyzed based on four angles: azimuthal angle, θ, and polar angle, φ, of both the particle length and width in a spherical coordinate system (Figure 5). Particle length and width correspond to the longest and shortest Feret diameters, respectively. In Avizo, the definition of Feret diameter is extended to three dimensions (3D), representing the distance between two parallel planes restricting the particle perpendicular to that direction. Avizo allows measurements of Feret diameters at various angles in 3D to determine the length and width of particles, and extracts their orientations. Analyzing the changes of the four angles enables the detection of particle rotation in all directions in 3D.

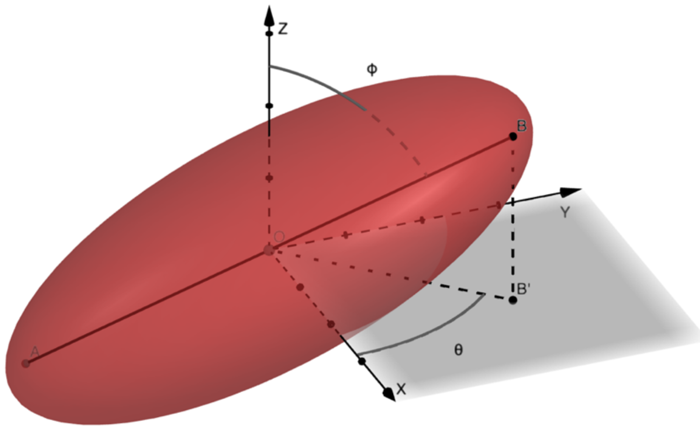

Figure 5: Illustration of spherical coordinates for rotation detection. For each particle, azimuthal angle $\boldsymbol{\theta}$ and polar angle $\boldsymbol{\varphi}$ for both particle length and width are extracted. Example is shown for particle length. The X, Y, Z axis directions refer to the original image axes since the influences of container tilt ($< \mathbf{0.1}°$) is negligible on rotation detection.

2.5.5 Particle contacts

Particle contact searching was performed on a labeled voxel field output from Avizo (Figure 6). In the labeled voxel field, each voxel was labeled with a particle label index (i.e., 1, 2, 3, …) or a void label (i.e., 0). The labeled voxel field was divided into small search windows. If the label indexes of two different particles appeared within the same search window, the two particles were considered to be in contact. To account for potential errors from the images and processing, two different window cubic sizes, 3 and 6 voxels, were used for contact searching. Contacts detected with the 3-voxel window were classified as close contacts, whereas additional contacts found using the 6-voxel window were classified as loose contacts. The coordination number was calculated by averaging the number of contacts for each individual particle.

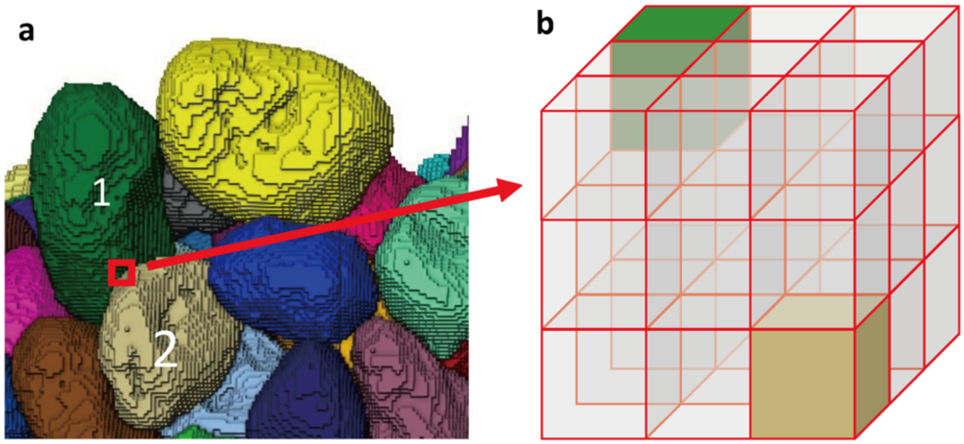

Figure 6: Contact detection by voxel window searching. The labeled voxel field is divided into small windows with a cubic size of 3 or 6 for searching particle contacts. (a) Labeled voxel field with particle indexes or void. (b) Example of detected close contact in a window with a cubic size of 3.

2.6 Reproducibility

The experiments were repeated three times, leading to very similar results (e.g., with mean deviation of volumetric strain upon each thermal cycle < 0.01% and more scattered dots compared to the results of angular particles). This reproducibility highlights the consistency and reliability of the results.

3. Results and discussion

3.1 Behavior upon the first cycle of heating and cooling

Figure 7 presents qualitative representations of the particle temperatures and quantitative assessments of particle vertical translations upon the completion of the first heating ramp and cooling ramp (the data reported via semi-transparent dots are de-emphasized because they are considered artifacts associated with image stitching and stage position control). The qualitative representation of the temperature field derived from the volume statistics reveals non-uniform temperature variations in the tested samples upon heating and cooling, which are attributed to a non-uniform gas flow in the temperature-controlled polymer cell. The particle vertical translations further indicate that particles move upward upon heating and downward upon cooling, with particles located at shallower depths experiencing larger translations compared to particles located at deeper depths. Particle translations accumulate with distance from the origin of the coordinate system, located at the bottom of the sample (e.g., upper particles are pushed further upwards by particles below during heating).

Temperature variations induce non-uniform particle vertical translations within the sample (depicted as scattered dots at certain heights), indicating the occurrence of relative sliding between particles. Particles located at shallower depths exhibit more freedom in rearranging and show a larger range of vertical translations due to the lower restraint compared to that at deeper locations. While the non-uniformity of the particle temperatures may contribute to the observed non-uniformity particle translations, its impact is expected to be secondary.

The shape of the particles strongly influences the magnitude of their translations. Firstly, this is evident from the overall slopes of the particle vertical translations in relation to the sample height, reflecting the magnitudes of the thermally induced volumetric strain. Secondly, the particle shape effect can be noted by looking at the scatter in the particle vertical translations at any given sample height, indicating relative sliding between the particles. Sands with rounded particles show larger magnitudes of particle translations and more significant particle sliding compared to angular sands, consistent with previous experimental evidence that showed larger macroscopic thermally induced strains in sands with rounded particles compared to angular particles [30]. This result is attributed to the reduced friction and rolling resistance characterizing rounded particles, which facilitate their mobility through less substantial restraints on particle movements.

The dominant upward particle translations observed upon heating suggest that the sands expand macroscopically. In other words, the results indicate no thermal collapse (i.e., volumetric contraction upon heating), corroborating recent evidence [26, 30, 44] as opposed to some previous studies [18, 23, 32, 10, 8, 28]. Upon cooling, the dominant downward particle translations suggest macroscopic contraction, whose magnitude is smaller than the expansion induced by heating.

The actual particle translations are generally bounded by the thermoelastic displacements derived from the volume statistics as well as the linear and volumetric thermal expansion of the solid particles. On the one hand, the magnitudes of particle vertical translations are smaller than the pink and gray dots, representing the thermoelastic displacements inferred from the measured volumes and volumetric thermal expansion coefficient of the particles, respectively. This result is attributed to constraints on particle translations resulting from friction and rolling resistance. On the other hand, the magnitudes of particle vertical translations generally surpass the blue dots, representing the thermoelastic displacements inferred from the linear thermal expansion coefficient of alpha quartz. This response is attributed to a boundary effect provided by the lateral restraint of the sample container. As the thermal expansion of the sample is partly restrained by the boundaries along the horizontal direction, a portion of the volume changes caused by the applied temperature variations is released in the vertical direction. This phenomenon leads to increased particle vertical translations in response to temperature variations and thermally induced vertical strains that are larger than those associated with the theoretical linear thermal expansion.

The thermoelastic displacements calculated through volume statistics by equation (1) show a consistent pink slope across the height, as well as comparable pink slopes upon heating and cooling. The trend of these thermoelastic displacements from equation (1) aligns closely with those derived from the volumetric thermal expansion coefficient of the particles (equation (2)). These comparisons validate the results obtained through particle volume statistics and the effectiveness of temperature control. However, some discrepancies between these results are noticed, which is likely due to limitations in the stitching of the images, as well as the spatial and temporal non-uniformity of the imposed temperature variations. For example, in the upper section of the samples, the thermoelastic displacements deriving from the volume statistics (pink) exhibit a slightly larger slope along the sample height compared to the lower sections. This is likely because temperature variations in the upper particles exceed 100 °C. The calibrated sample temperature primarily reflects the temperature of lower particles, whereas the temperature of upper particles in closer proximity to the heater is expected to be slightly higher.

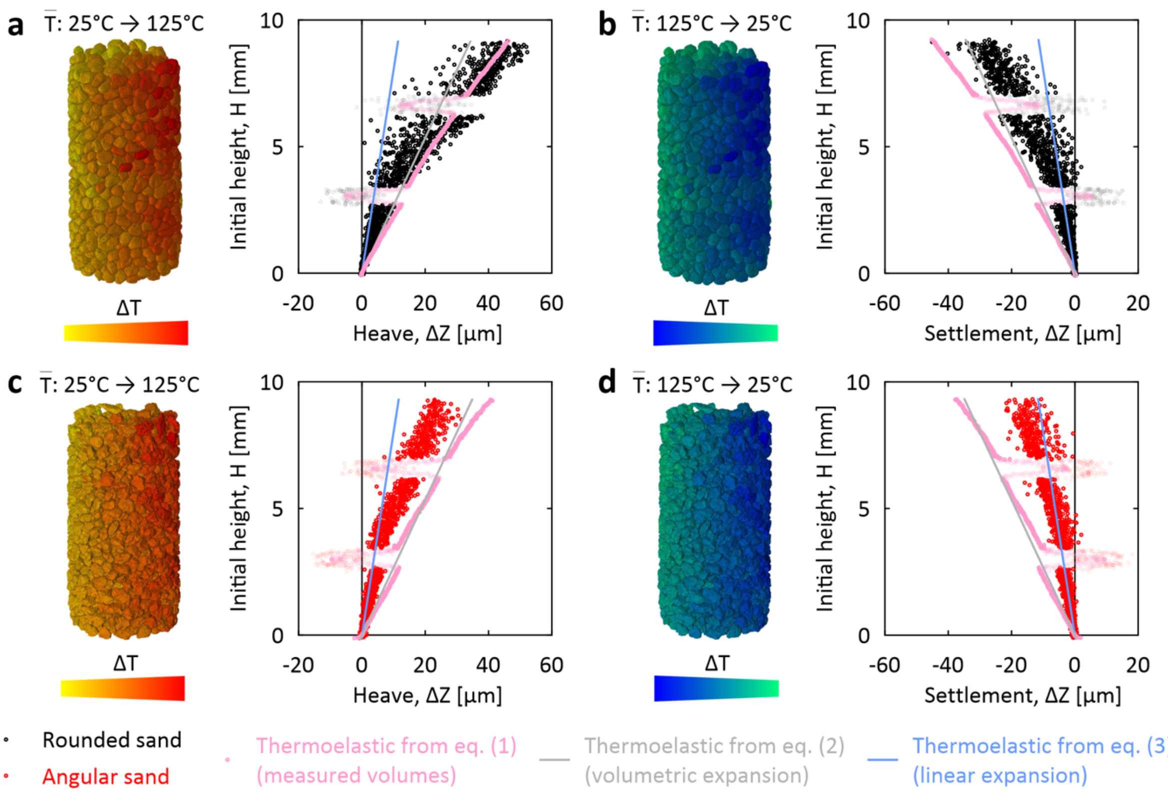

Figure 7: Particle vertical translations against the initial height and temperature variation field upon first cycle of heating and cooling. Qualitative temperature variation fields based on measured thermal expansion/contraction of individual particles (i.e., volume variation percentage $\Delta \boldsymbol{V_s^m}/\boldsymbol{V_{s,i}^m}$ where $\boldsymbol{V_s^m}$ represents solid volume in CT images) are visualized by rendering with colormap. The colors of particles around image stitches are corrected by averaging and rescaling colors of neighbor particles. Each black or red dot represents the vertical translation $\Delta \boldsymbol{Z}$ of one particle at its height $\boldsymbol{H}$. Pink dots are related to the displacement distribution inferred from the measured thermal expansion/contraction of the sum of particle volumes below a given height. Gray lines represent the displacement distribution of the theoretical volumetric thermal expansion/contraction ($\Delta \boldsymbol{T} = \pm \boldsymbol{100}$ °C) of alpha quartz across the sample height $\boldsymbol{H}$, considering zero lateral strains. Blue lines represent the displacement distribution of the theoretical linear thermal expansion/contraction ($\Delta \boldsymbol{T} = \pm \boldsymbol{100}$ °C) of alpha quartz across the sample height $\boldsymbol{H}$. The shifts de-emphasized by semi-transparent dots at $\boldsymbol{H} \approx 3$ and 6 mm are associated with image stitching artifacts. (a) Rounded sand upon heating. (b) Rounded sand upon cooling. (c) Angular sand upon heating. (d) Angular sand upon cooling.

3.2 Behavior upon multiple cycles of heating and cooling

Figure 8 shows the particle translations upon the completion of each thermal cycle (no image stitching artifacts are present because the images were consistently taken at the same temperature). In general, the samples experience a net irreversible settlement of their particles upon the completion of each thermal cycle, which corresponds to a bulk macroscopic volumetric contraction of the material. The observed non-uniformity in particle vertical translations, suggesting an irreversible sliding between the particles, seems to contribute to a generally negative translation slope across the sample height after each thermal cycle. This negative translation slope corresponds to a volumetric contractive strain in the material.

This evidence is consistent with recent experimental observations reported for sands subjected to thermal cycles in an oedometer apparatus [31], which report irreversible volumetric contractions due to thermal cycling. However, in contrast to these observations, the results obtained in the present work highlight an irreversible volumetric expansion of the samples after the first cycle. Notably, a similar transitional behavior was also reported in previous numerical simulations [24], with granular materials subjected to thermal cycling that initially exhibited residual macroscopic expansions followed by residual volumetric contractions in subsequent cycles. The net residual heave of granular particles upon the completion of the first thermal cycle in Figure 8 directly results from smaller downward particle translations upon cooling compared to the upward translations observed upon heating during the first cycle (see Figure 7). This evidence is unlikely due to an incomplete cooling of the tested granular materials, because the comparable pink slopes upon heating and cooling in Figure 7 indicate comparable thermal expansion and contraction of the measured particle volumes, as well as a coherent temperature profile before and after the first thermal cycle.

Overall, sands with rounded particles exhibit larger volumetric deformations compared to sands with angular particles upon the successive application of thermal cycles, confirming that particle shape strongly influence the constraints that characterize any granular packing. This response is in agreement with recent experimental findings on sands subjected to thermal cycles in an oedometer apparatus, which also noted that irreversible deformations caused by thermal cycling decrease with an higher applied stress level and the initial relative density [31]. However, this behavior contrasts with the response of sands under compressive stresses, where sands with more angular particles are known to be more porous and hence deformable (at a given relative density) compared to sands with more rounded particles [48]. The different role of particle shape in the deformation of granular materials subjected to temperature variations and external stresses is attributed to the distinct mechanisms involved, resulting from imposed deformations and forces, respectively.

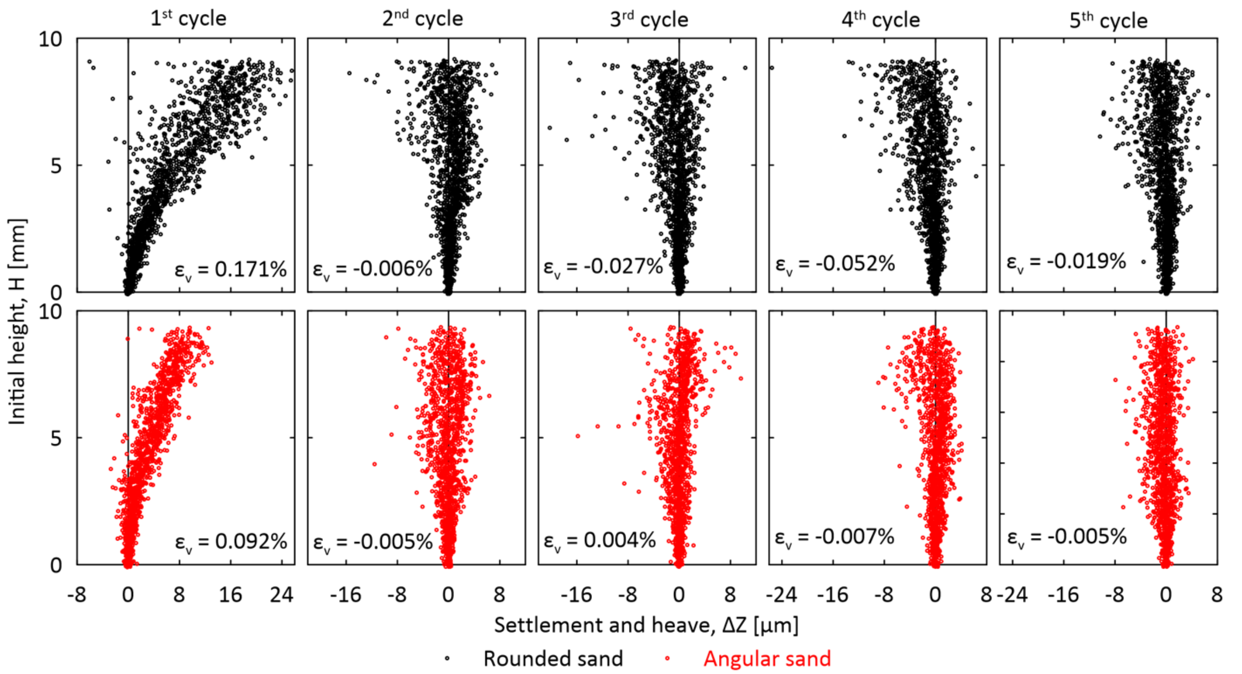

Figure 8: Particle vertical translations upon each thermal cycle. Each black or red dot represents the vertical translation $\Delta \boldsymbol{Z}$ of one particle at its height $\boldsymbol{H}$. Volumetric strains $\boldsymbol{\varepsilon_v}$ are calculated by dividing the average vertical displacement of top layer particles by their average initial height.

Figure 9 illustrates the effects of thermal cycling on particle rotations and contact variations in granular materials. Overall, particle rotations and contact variations are more pronounced in granular materials with rounded particles compared to angular particles. The percentage of rounded particles that rotate upon each thermal cycle ranges from 11% to 13% (Figure 9(a)), whereas the percentage of angular particles that rotate upon each thermal cycle ranges from 6% to 10% ($\Delta\theta > 0.5°$, $\Delta\varphi > 0.1°$). When considering the variations in coordination numbers along with the number of applied thermal cycles (Figure 9(b)), the results indicate that, on average, each rounded particle is initially in contact with approximately 7.3 neighbor particles, while each angular particle is in contact with approximately 6.6 neighbor particles. This finding is consistent with the lower porosity and more regular surfaces of rounded particles. The results suggest that the total particle contacts increase cycle after cycle in sand with rounded particles, whereas the contacts among angular particles remain relatively constant over the considered number of cycles. The first thermal cycle appears to yield a loss of some close contacts for both sands (as seen in the initial irreversible expansion in Figure 8), followed by a gradual increase of close contacts in subsequent cycles.

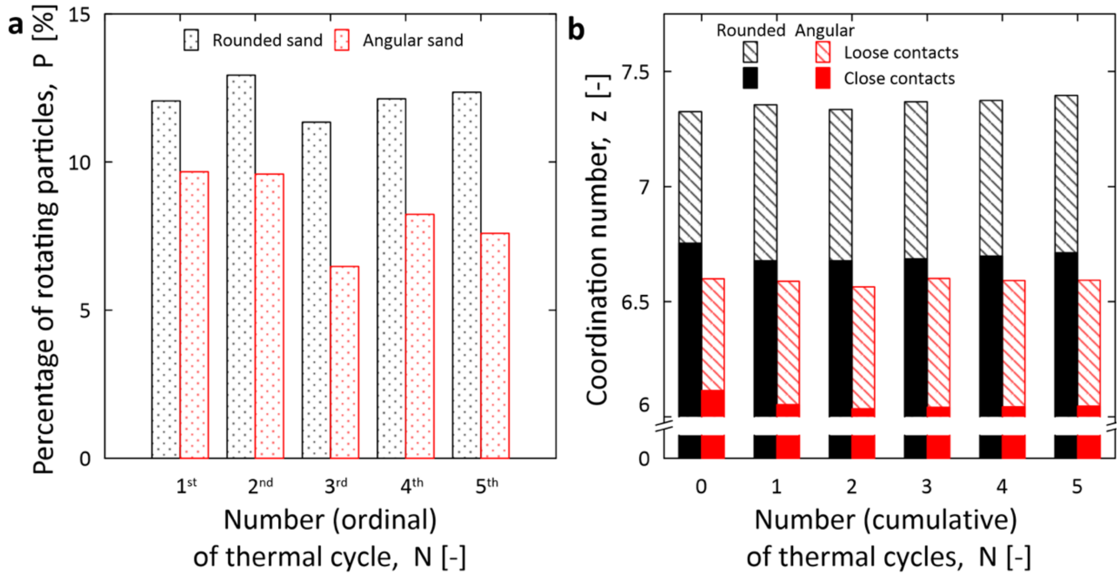

Figure 9: Particle rotations and contact variations induced by thermal cycling. (a) Percentages of rotating particles $\boldsymbol{P}$ detected during each thermal cycle. The rotation of each particle is detected by checking 4 angles in total including the polar angle $\boldsymbol{\theta}$ and azimuthal angle $\boldsymbol{\varphi}$ of both particle length and width. Each data represents the change during each cycle. (b) Coordination number $\boldsymbol{z}$ along with the number of applied thermal cycles determined by voxel window searching. Close contacts are searched by a voxel window with a cubic size of 3. Loose contacts are searched by a voxel window with a cubic size of 6. Each data represents the current state in each image scan.

4. Closure

This paper provided unprecedented experimental evidence about the microscopic phenomena that govern the macroscopic deformations of granular materials subjected to cyclic temperature variations. This study specifically analyzed dry silica sands with different particle shapes, leveraging tomography experiments with ultra-bright, high-energy X-ray beams, and image analyses.

The results substantiate that the macroscopic deformations of granular materials subjected to temperature variations are driven by microscopic particle rearrangements, which originate from thermally induced particle deformations. These particle rearrangements encompass non-uniform particle translations (indicating relative sliding), rotations, and contact variations. They involve a volumetric expansion of granular materials upon heating and a volumetric contraction upon cooling, leading to irreversible macroscopic deformations upon successive thermal cycles.

The findings indicate that particle shape fundamentally influences the microscopic particle interactions in granular materials upon thermal cycling. Granular materials with angular particles undergo less significant particle translations, rotations, and contact variations for any applied temperature variations compared to materials with rounded particles. Additionally, the particle vertical translations observed in granular materials with angular particles tend to be more uniform compared to those in materials with rounded particles. This is primarily due to the larger interlocking and inherent constraint characteristic of angular particle materials compared to rounded particle materials. Specifically, this evidence arises from the lesser friction and rolling resistance of rounded particles, which possess smoother surfaces, higher sphericity, and greater roundness compared to angular particles.

Taken together, the results of this study offer previously unavailable experimental evidence regarding the microscopic origins of thermally induced deformations in granular materials. Consequently, this study represents an advancement in understanding the mechanics of granular materials under non-isothermal conditions – a topic of central importance in the context of various problems in science, engineering, and technology.

Declarations

Competing interest

The authors have no competing interests to declare that are relevant to the content of this article.

Authors contributions

YP performed and analyzed the experiments, created the figures, and wrote the manuscript. DS provided technical support for the image analyses and revised the manuscript. MR built the experimental setup, provided technical support at the beamline facility, and revised the manuscript. XG performed some of the experiments. GB provided the tools to perform the image analyses, contributed to the interpretation of the results, and revised the manuscript. AFRL conceptually developed and supported the research and wrote and revised the manuscript.

Data availability

Correspondence and requests for materials should be addressed to AFRL. Processed data available on request from AFRL.

Acknowledgments

This research was partly supported by the United States Army Research Office (project grant W911NF2110059) and the United States National Science Foundation (project grant No. 2046586). This research used resources of the Advanced Photon Source, a U.S. Department of Energy (DOE) Office of Science User Facility operated for the DOE Office of Science by Argonne National Laboratory under Contract No. DE-AC02-06CH11357. We acknowledge the support of GeoSoilEnviroCARS (The University of Chicago, Sector 13), Advanced Photon Source (APS), Argonne National Laboratory. GeoSoilEnviroCARS is supported by the National Science Foundation – Earth Sciences (EAR – 1634415).

References

1. Corwin, E.I., Jaeger, H.M., Nagel, S.R.: Structural signature of jamming in granular media. Nature. 435, 1075–1078 (2005)
2. Kou, B., Cao, Y., Li, J., Xia, C., Li, Z., Dong, H., Zhang, A., Zhang, J., Kob, W., Wang, Y.: Granular materials flow like complex fluids. Nature. 551, 360–363 (2017)
3. Deal, E., Venditti, J.G., Benavides, S.J., Bradley, R., Zhang, Q., Kamrin, K., Perron, J.T.: Grain shape effects in bed load sediment transport. Nature. 613, 298–302 (2023). https://doi.org/10.1038/s41586-022-05564-6
4. Jaeger, H.M., Shinbrot, T., Umbanhowar, P.B.: Does the granular matter? Proceedings of the National Academy of Sciences. 97, 12959–12960 (2000). https://doi.org/10.1073/pnas.230395897
5. Kawamoto, R., Andò, E., Viggiani, G., Andrade, J.E.: All you need is shape: Predicting shear banding in sand with LS-DEM. Journal of the Mechanics and Physics of Solids. 111, 375–392 (2018). https://doi.org/10.1016/j.jmps.2017.10.003
6. Seo, D., Sohn, C., Cil, M.B., Buscarnera, G.: Evolution of particle morphology and mode of fracture during the oedometric compression of sand. Géotechnique. 71, 853–865 (2021). https://doi.org/10.1680/jgeot.18.P.300
7. Yan, W.M., Dong, J.: Effect of Particle Grading on the Response of an Idealized Granular Assemblage. International Journal of Geomechanics. 11, 276–285 (2011). https://doi.org/10.1061/(ASCE)GM.1943-5622.0000085
8. Kosar, K.M.: The effect of heated foundations on oil sand, (1983)
9. Manbeck, H.B.: Predicting thermally induced pressures in grain bins. Transactions of the ASAE. 27, 482–0486 (1984)
10. Agar, J.G., Morgenstern, N.R., Scott, J.D.: Thermal-expansion and pore pressure generation in oil sands. Can. Geotech. J. 23, 327–333 (1986)
11. Chen, K., Cole, J., Conger, C., Draskovic, J., Lohr, M., Klein, K., Scheidemantel, T., Schiffer, P.: Granular materials: Packing grains by thermal cycling. Nature. 442, 257 (2006)
12. Vargas, W.L., McCarthy, J.J.: Thermal expansion effects and heat conduction in granular materials. Physical Review E. 76, 041301 (2007)
13. Divoux, T., Gayvallet, H., Géminard, J.-C.: Creep Motion of a Granular Pile Induced by Thermal Cycling. Phys. Rev. Lett. 101, 148303 (2008). https://doi.org/10.1103/PhysRevLett.101.148303

14. Dreissigacker, V., Müller-Steinhagen, H., Zunft, S.: Thermo-mechanical analysis of packed beds for large-scale storage of high temperature heat. Heat and Mass Transfer. 46, 1199–1207 (2010). https://doi.org/10.1007/s00231-010-0684-5
15. Dreißigacker, V., Zunft, S., Müller-Steinhagen, H.: A thermo-mechanical model of packed-bed storage and experimental validation. Applied Energy. 111, 1120–1125 (2013). https://doi.org/10.1016/j.apenergy.2013.03.067
16. Percier, B., Divoux, T., Taberlet, N.: Insights on the local dynamics induced by thermal cycling in granular matter. EPL (Europhysics Letters). 104, 24001 (2013). https://doi.org/10.1209/0295-5075/104/24001
17. Zhao, S., Evans, T.M., Zhou, X., Zhou, S.: Discrete element method investigation on thermally-induced shakedown of granular materials. Granular Matter. 19, (2016). https://doi.org/10.1007/s10035-016-0690-5
18. Ng, C.W.W., Wang, S.H., Zhou, C.: Volume change behaviour of saturated sand under thermal cycles. Géotechnique Letters. 6, 124–131 (2016)
19. McCartney, J.S., Xiao, Y., Liu, H., Liu, H.: Influence of temperature on the volume change behavior of saturated sand. Geotechnical Testing Journal. 41, (2018)
20. Sassine, N., Donzé, F.-V., Harthong, B., Bruch, A.: Thermal stress numerical study in granular packed bed storage tank. Granular Matter. 20, 1–15 (2018)
21. Knödler, P.: Thermo-Mechanical Investigations of Packed Beds for High Temperature Heat Storage: Uniaxial Compression Test Experiments and Particle Discrete Simulations. Applied Sciences. 9, (2019). https://doi.org/10.3390/app9081600
22. Iliev, P.S., Giacomazzi, E., Wittel, F.K., Mendoza, M., Haselbacher, A., Herrmann, H.J.: Behavior of confined granular beds under cyclic thermal loading. Granular Matter. 21, 59 (2019). https://doi.org/10.1007/s10035-019-0914-6
23. Sittidumrong, J., Jotisankasa, A., Chantawarangul, K.: Effect of thermal cycles on volumetric behaviour of Bangkok sand. Geomechanics for Energy and the Environment. 100127 (2019). https://doi.org/10.1016/j.gete.2019.100127
24. Zhao, S., Zhao, J., Lai, Y.: Multiscale modeling of thermo-mechanical responses of granular materials: A hierarchical continuum–discrete coupling approach. Computer Methods in Applied Mechanics and Engineering. 367, 113100 (2020). https://doi.org/10.1016/j.cma.2020.113100
25. Mitterlehner, T., Kartnig, G., Haider, M.: Analysis of the thermal ratcheting phenomenon in packed-bed thermal energy storage using discrete element method. FME Transactions. 48, 427–431 (2020)
26. Pan, Y., Coulibaly, J.B., Rotta Loria, A.F.: Thermally induced deformation of coarse-grained soils under nearly zero vertical stress. Géotechnique Letters. 10, 486–491 (2020). https://doi.org/10.1680/jgele.20.00013
27. Coulibaly, J.B., Shah, M., Rotta Loria, A.F.: Thermal cycling effects on the structure and physical properties of granular materials. Granular Matter. 22, 80 (2020). https://doi.org/10.1007/s10035-020-01054-6
28. He, S.-H., Shan, H.-F., Xia, T.-D., Liu, Z.-J., Ding, Z., Xia, F.: The effect of temperature on the drained shear behavior of calcareous sand. Acta Geotech. 16, 613–633 (2021). https://doi.org/10.1007/s11440-020-01030-7
29. Coulibaly, J.B., Rotta Loria, A.F.: Transient dynamics of the thermally induced deformation of sands. International Journal for Numerical and Analytical Methods in Geomechanics. 46, 1972–1988 (2022)
30. Pan, Y., Coulibaly, J.B., Rotta Loria, A.F.: An experimental investigation challenging the thermal collapse of sand. Géotechnique. 1–27 (2022)
31. Pan, Y., Gong, X., Rotta Loria, A.F.: Thermal shakedown in granular materials with irregular particle shapes. Scientific Reports. 14, 6828 (2024). https://doi.org/10.1038/s41598-024-57503-2
32. Agar, J.G.: Geotechnical behaviour of oil sands at elevated temperatures and pressures, (1984)

33. Laloui, L., Rotta Loria, A.F.: Analysis and Design of Energy Geostructures: Theoretical Essentials and Practical Application. Academic Press (2019)
34. Carson, J.W.: Silo failures: Case histories and lessons learned. Handbook of Powder Technology. 10, 153–166 (2001)
35. Dogangun, A., Karaca, Z., Durmus, A., Sezen, H.: Cause of Damage and Failures in Silo Structures. Journal of Performance of Constructed Facilities. 23, 65–71 (2009). https://doi.org/10.1061/(ASCE)0887-3828(2009)23:2(65)
36. Slotterback, S., Toiya, M., Goff, L., Douglas, J.F., Losert, W.: Correlation between Particle Motion and Voronoi-Cell-Shape Fluctuations during the Compaction of Granular Matter. Phys. Rev. Lett. 101, 258001 (2008). https://doi.org/10.1103/PhysRevLett.101.258001
37. Alonso-Marroquín, F., Herrmann, H.J.: Ratcheting of Granular Materials. Phys. Rev. Lett. 92, 054301 (2004). https://doi.org/10.1103/PhysRevLett.92.054301
38. García-Rojo, R., Herrmann, H.J.: Shakedown of unbound granular material. Granular Matter. 7, 109–118 (2005). https://doi.org/10.1007/s10035-004-0186-6
39. McNamara, S., García-Rojo, R., Herrmann, H.J.: Microscopic origin of granular ratcheting. Phys. Rev. E. 77, 031304 (2008). https://doi.org/10.1103/PhysRevE.77.031304
40. Cuéllar, P., Baeßler, M., Rücker, W.: Ratcheting convective cells of sand grains around offshore piles under cyclic lateral loads. Granular Matter. 11, 379 (2009). https://doi.org/10.1007/s10035-009-0153-3
41. Park, J., Santamarina, J.C.: Sand response to a large number of loading cycles under zero-lateral-strain conditions: evolution of void ratio and small-strain stiffness. Géotechnique. 69, 501–513 (2019)
42. Rivers, M.L.: tomoRecon: High-speed tomography reconstruction on workstations using multi-threading. In: Developments in X-Ray Tomography VIII. p. 85060U. International Society for Optics and Photonics (2012)
43. Rivers, M.L.: High-speed tomography using pink beam at GeoSoilEnviroCARS. Presented at the Proc.SPIE (2016)
44. Pan, Y., Seo, D., Rivers, M., Buscarnera, G., Rotta Loria, A.F.: Computed Tomography of Sand Subjected to Heating: Analysis of Particle Displacements. 435–444 (2023). https://doi.org/10.1061/9780784484678.044
45. Vaid, Y.P., Negussey, D.: Preparation of Reconstituted Sand Specimens. Advanced Triaxial Testing of Soil and Rock. (1988). https://doi.org/10.1520/STP29090S
46. Coulibaly, J.B., Rotta Loria, A.F.: Thermally induced deformation of soils: A critical revision and update of experimental analyses. Geotechnical Testing Journal. under review, (2023)
47. Kosinski, J.A., Gualtieri, J.G., Ballato, A.: Thermal expansion of alpha quartz. In: Proceedings of the 45th Annual Symposium on Frequency Control 1991. pp. 22–28. IEEE, Los Angeles, CA, USA (1991)
48. Cho, G.-C., Dodds, J., Santamarina, J.C.: Particle Shape Effects on Packing Density, Stiffness, and Strength: Natural and Crushed Sands. Journal of Geotechnical and Geoenvironmental Engineering. 132, 591–602 (2006). https://doi.org/10.1061/(ASCE)1090-0241(2006)132:5(591)